Eur. Phys. J. E (2020) **43**: 45
DOI 10.1140/epje/i2020-11970-y

THE EUROPEAN PHYSICAL JOURNAL E

Regular Article

Thermoelectric effects induced dendrite branching dynamics in pure substances: An insight from morphological theory*

Limei Fu[1], Youqi Cao[2], Zhongtang Gao[3], Lihong Dong[1], and Lifei Du[2,a]

[1] College of Computer Science and Technology, Xi'an University of Science and Technology, Xi'an 710054, P.R. China
[2] College of Materials Science and Engineering, Xi'an University of Science and Technology, Xi'an 710054, P.R. China
[3] College of Mechanical Engineering, Xi'an University of Science and Technology, Xi'an 710054, P.R. China

Received 31 March 2019 and Received in final form 29 February 2020
Published online: 9 July 2020

Abstract. Insights on the mechanical behavior in materials highly depend upon sufficiently characterizing microstructure details at the relevant length scales. In this study, the side-branching dynamics of dendritic structures formation in pure substances is studied upon the phase-field simulations of crystallization with applied direct currents. The effect of heat diffusion (including thermoelectric effect and undercooling) on the dendritic development is investigated, and the characteristics of the primary arms and side-branches are identified by implementing the image recognition technique. Results indicate that increasing the latent heat release would firstly enhance the side-branching and then cause the side-branches re-melting with large heat extraction form the solid. The side-branching could be tailored by rationally controlling the applied electric filed as well the heat treatment, which could be a potential way to improve the mechanical properties in metallic materials via optimizing the microstructure.

1 Introduction

Dendrite structures, which are highly hierarchical branched patterns with primary-, secondary- and higher-order branches, are of immense practical importance in determining the engineering properties of materials that solidify dendritically [1–3]. Studying the dendritic growth has also been of long-standing fundamental interest because of the ubiquity of branched structures exhibited by diverse interfacial pattern formation systems, and discovering how crystals grow, develop, and create such complex patterns has been a challenge to researchers in crystalline materials for several centuries [4–10]. Considering the crystallization from liquids should be mostly determined by the heat and solute diffusions at the interfaces, the crystalline microstructure should be the result of the morphological instability of the solid-liquid interface. It has been well established that the phase stability during crystallization in pure substances is mostly dependent on the temperature gradient at the solid-liquid interface, and the growth rate should be determined by the level of the latent heat diffusing away from the solid-liquid interface [11]. The effect of the heat flux on the microstructure formation in crystalline materials has been well studied [12], which achieves clear relationships between morphology of dendrites, solute diffusion and heat diffusion. Most recently, applying the electric field during metallic solidification became a promising way to control and modify the solidification process in order to optimize the microstructures [13–15]. Due to thermal phenomena which includes Joule, Peltier and Thomson effects, etc., heat may be emitted or absorbed during crystal solidification with an electric current passing through the sample [16–19]. It is has been proved that for different pure substances (Sn and Bi), the dendritic morphology shows different side-branching characteristics with applied electric field. The reason for these structural differences is believed to be correlated to the thermal effect induced by the electric field, since the heat distributions near the interfaces would be more complicated with the applied electric field [19]. Thus, it is of great importance to characterize the microstructure, especially the side-branching characteristics, formed with applied electric field, in order to give insights on the electromagnetic solidification process control. In this study, the heat effect (including latent heat and thermoelectric effects) on the dendritic branching dynamics during the rapid undercooled solidification with applied current would be carried out by implementing the phase-field simulation, and the characteristics of the solidifying

* Contribution to the Topical Issue "Branching Dynamics at the Mesoscopic Scale" edited by Yongsheng Han, Hui Xing, Dongke Sun.

[a] e-mail: dulifei@xust.edu.cn (corresponding author)

dendritic structures would be statistically identified based on the image recognition technique, which would give an insight of the branching dynamics and pattern selection mechanisms for crystallizing with the electric field.

2 Phase-field modeling and simulation

Based on the model for dendrite growth in pure substances with applied direct current [19], the governing equation for the phase-field variable $\phi(\boldsymbol{r}, t)$ (in solid phase $\phi = 1$, in liquid phase $\phi = 0$) is

$$\tau_\phi \frac{\partial \phi}{\partial t} = \phi\,(1-\phi)\left(\phi - \frac{1}{2} + m + a\chi\right) + \nabla\cdot\left(\varepsilon^2\nabla\phi\right) - \frac{\partial}{\partial x}\left(\varepsilon\varepsilon'\frac{\partial\phi}{\partial x}\right) + \frac{\partial}{\partial y}\left(\varepsilon\varepsilon'\frac{\partial\phi}{\partial y}\right). \quad (1)$$

To involve the electric field into the solidification, the description of heat flux $\boldsymbol{q}$ and electric current density $\boldsymbol{J}$ is modified as follows to incorporate the thermo-electric effects [11]: Fourier law: $\boldsymbol{q} = -\kappa\nabla T + ST\boldsymbol{J}$; Ohm's law: $\boldsymbol{J}/\sigma = -\nabla\varphi + \boldsymbol{u}\times\boldsymbol{B} - S\nabla T$, where κ and σ are the heat conductivity and electric conductivity, respectively. T is the temperature. S is the absolute thermo-electric power. $\boldsymbol{J}$ and φ are the electric current density and electric potential, respectively. $\boldsymbol{B}$ is the magnetic field.

The electric potential φ is described by

$$\nabla\cdot(\sigma\nabla\varphi) = 0. \quad (2)$$

Considering that a steady-state electric field is imposed in specific direction for all simulations, the energy equation for heat diffusion involving thermoelectric effects can be written as

$$\frac{\partial}{\partial t}(\rho C T) = \nabla\cdot(\kappa\nabla T) + \frac{J^2}{\sigma} - \tau J\cdot\nabla T + \pi J + K\frac{\partial\phi}{\partial t}, \quad (3)$$

where ρ is the density, C is the heat capacity, κ is the heat conductivity, J represents the current density, σ is the electric conductivity, $\tau = T\,\mathrm{d}S/\mathrm{d}T$ is the Thomson coefficient, π is the Peltier coefficient which should be a continuous function of the phase-field ($\pi = [(1-\phi)s_\mathrm{L} - \phi s_\mathrm{S}]T_\mathrm{M}$; s_L and s_S are Seebeck coefficients for the liquid and solid phase, respectively, and T_M is the melting temperature), and $K = \rho C L/c_p\Delta T$ is the dimensionless latent heat, which is proportional to the latent heat (L) and inversely proportional to the strength of the undercooling (ΔT). Terms on the right side of eq. (3) represent the heat conduction, Joule heat, Thomson effect, Peltier effect and latent heat (undercooling), respectively. Equations (1) and (3) are solved via the finite difference method, and zero-flux boundary conditions which are applied for both phase-field variable and temperature field. A steady-state electric field is imposed and not solved in this study, since we only focus on the thermo effect induced by applied direct current densities. Since the heat diffusion is highly correlated to the current direction as well as the physical property differences between the solid and liquid phase, solidification of two different pure substances (Sn and Bi) is simulated in this study, and parameter values for the simulations can be found in ref. [20].

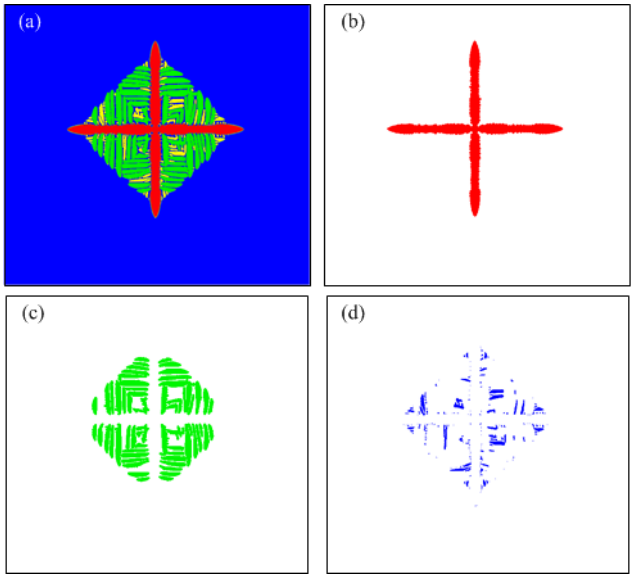

Fig. 1. Schematic diagram of image recognition process for branches in dendrites. (a) feature recognition; (b) primary arm; (c) secondary branches; (d) tertiary branches.

As shown in fig. 1, in order to precisely characterize the microstructure formed under different conditions, the image identification and data statistics are carried out for all simulation results: 1) The primary branches of the dendrite are identified through image corrosion and expansion algorithm, and the area, length, width and tip curvature of the primary dendrite arms are calculated; 2) the difference quotient diagrams of the primary branches and whole dendrite are calculated, and the Hausdorff distances between the residual dendrite and the primary branches in the difference quotient diagram are calculated; 3) the second-order branches are identified through the minimum threshold segmentation, and the total area and number of the secondary-order branches as well as the Hausdorff distances between different second-order branches are calculated; 4) the high-order branches are identified by subtracting the second-order branches with the difference quotient diagram in the second step, and finally the number and area of the third-order branches are calculated. With these extracted data from image processing, the side-branching dynamics of the pure substances could be analyzed and discussed.

3 Results and discussions

It has been discussed in ref. [19] that with induced current during the solidification in pure Sn and Bi, the dendrite formatting process would be changed in different patterns with increasing current density ($\mathrm{A/m^2}$). As shown in fig. 2, the morphology of the dendritic microstructure achieved form the numerical simulations with different K and J at the same time shows obvious different branching characteristics, and the aim for this study is to under-

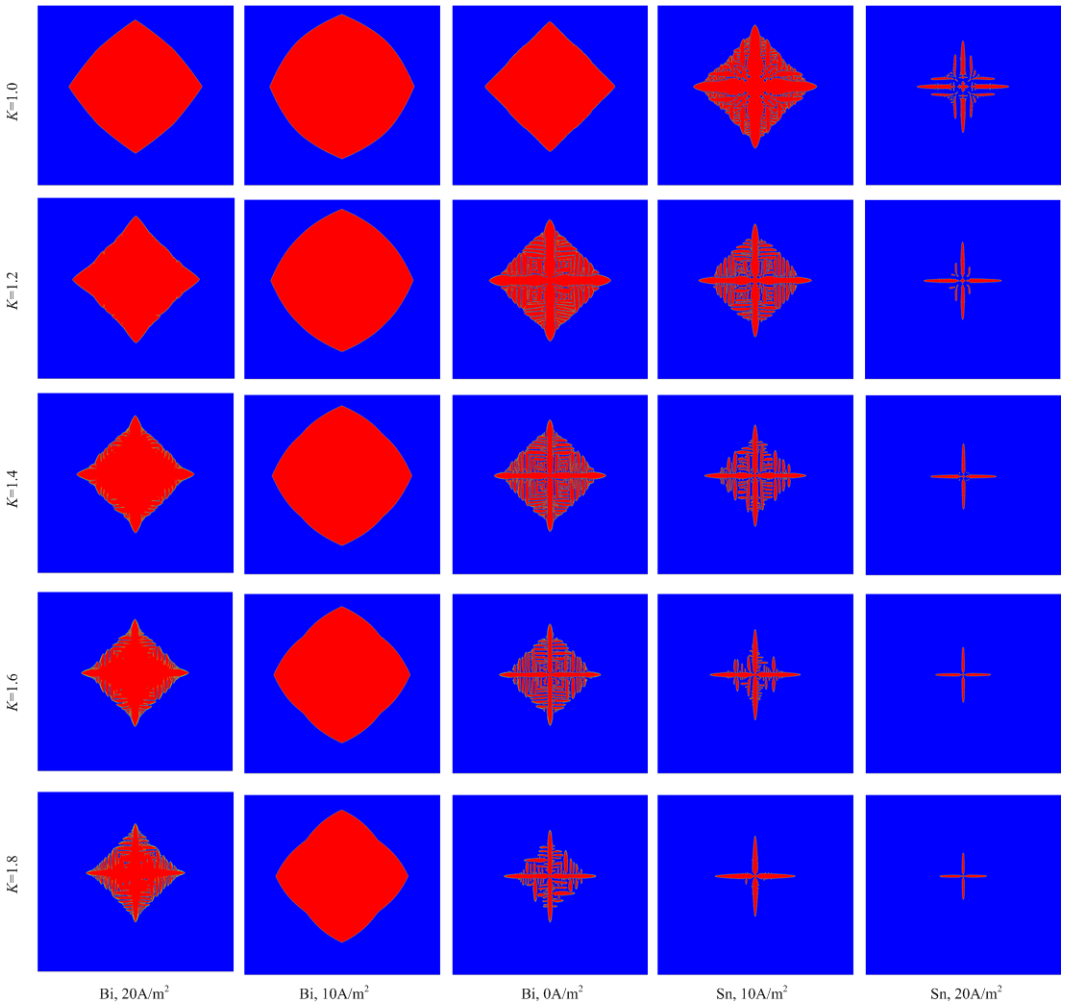

Fig. 2. Dendrite morphology formed form the pure metal melt with applied current under different undercooling.

stand the morphology transition mechanisms induced by the thermoelectric effects based on quantitatively specifying the dendritic microstructure. It is established that microstructure changes during crystallization are directly attributable to the temperature gradient in the growing direction. Thus, besides the Joule heat, Thomson heat and Peltier heat induced from the applied current, the undercooling during the liquid-solid transition also plays a significant role on the liquid-solid interface stability during the crystallization, which should also be considered [9].

As shown in fig. 2, the morphology of the dendrite also shows very different characteristics with increasing K. Without applied DC, the morphologies for pure Bi and pure Sn are almost the same under different undercooling rate, thus in fig. 2, we only plot the dendrite morphology for Bi without applied current. It can be easily seen that applying current has obviously different effects on the morphologies for Bi and Sn. With the current density increasing, the Sn dendrite shows a strong side-branching activity transition: the side-branches are firstly enhanced with small J, then remelted with increasing J. For Bi, with increasing current densities, no side-branches would be developed, and the equiaxed grain changes to globular shape firstly and then changes back to equiaxed crystal. No side-branching activity is detected during solidification of Bi equiaxed grains. With increasing K for the liquid-solid phase transition, all the morphology formed during the solidification changes dramatically. The shape of the dendrite, including the primary arm, secondary and tertiary branches all change in different modes, leading to the obvious different characteristics of the microstructure. It should be firstly noticed that without current, the dendritic microstructure changes from the quadrilateral shape to the branching patterns as K increases, and the side-branches are firstly enhanced and then compromised with large K. With induced current, the dendrite morphology changes in different patterns, which has been systematically discussed in ref. [19], and the side-branching also changes in different way with increasing K.

In fig. 3, the solid rate (S_0, which is defined as the solid fraction of crystallization), the number of the secondary dendritic arms (N_2) and third dendritic arms (N_3) are stratified and plotted as a function of K for the different conditions shown in fig. 2. With increasing K, the solid rate decreases as the result of the decreased undercooling with large K. Appling current has obviously differ-

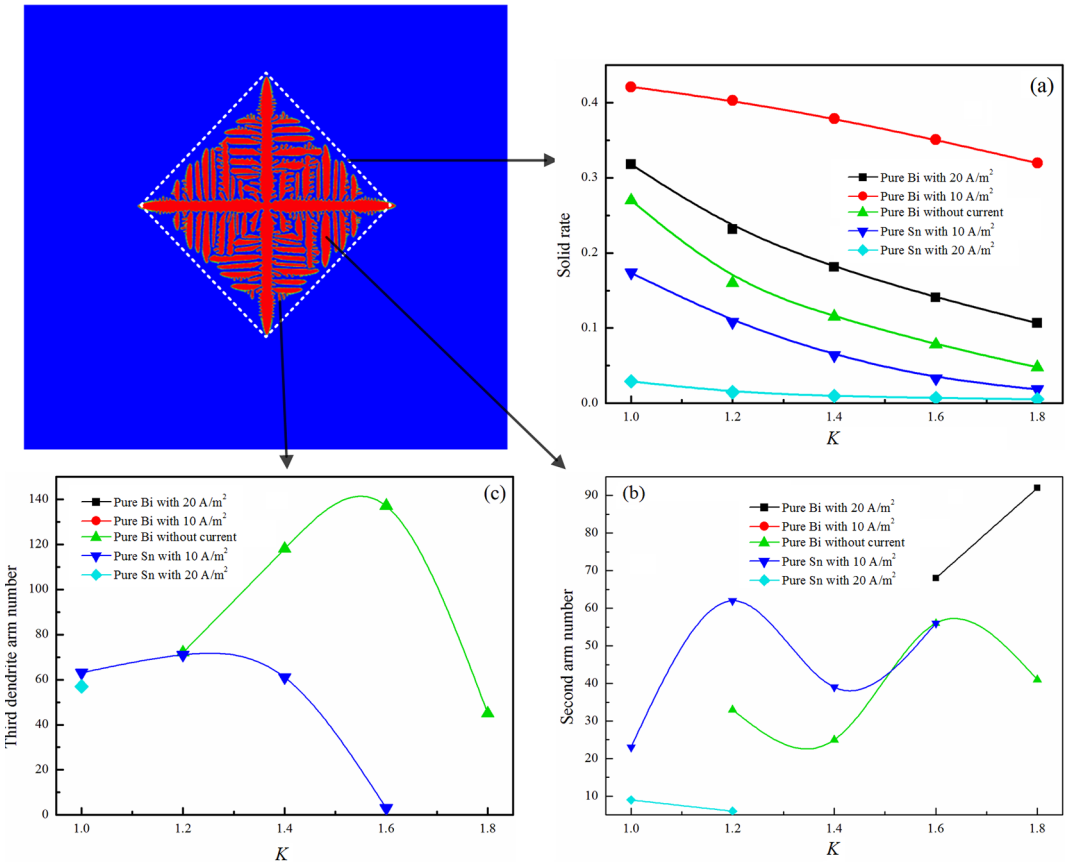

Fig. 3. Side-braches characteristics of the dendrites formed with applied current densities coupling with different K: (a) solid rate of the simulation zone; (b) number of secondary branches; (c) number of tertiary branches.

ent influences on the dendrite morphologies for Bi and Sn. With the current density increasing, the Sn dendrite shows a strong side-branching activity transition, while the equiaxed grain firstly changes to a globular shape with small direct current (DC), then changes back to an equiaxed shape. With small K, no side-branching activity is detected during solidification of Bi equiaxed grains, and the growth rate of the equiaxed grains is also greatly changed with different DC due to the large Joule heat generated from large current densities.

Secondary and tertiary branches are important insofar as they establish the length scales and patterns of the grains, which are of immense practical importance in determining the engineering properties of materials that solidify dendritically [1]. Thus, applying DC into crystallization might be an efficient way to adjust the dendritic morphology in pure substances. As shown in fig. 3, the side-branches are formed with specific current density and undercooling, and the numbers of second and third dendritic arms as a function of K are also plotted in fig. 3(b) and (c). Unlike the solid rate which decreases with increasing K, the numbers of the side-branches show nonlinear changes with increasing K, which would lead to a variety of microstructures with thermoelectric effects coupling with latent heat release. These results correspond to temperature distributions near the solid-liquid interface [19], which might provide a direct way to adjust the crystalline microstructure by controlling the temperature distributions.

Characterizing the primary dendrite arm in solidified microstructures is an important step for developing the relation between the processing and properties, since the shape of the primary arms is the highly correlated to the size of the grains form during solidifications [21]. As shown in fig. 4, the shape characteristics of the primary arms formed with different K during the solidification of pure Bi and Sn with different current densities is statistically identified. With increasing K, the length of the primary arm decreases and the tip curvature increases, which indicates the different forming speeds of the dendrite arm with different temperature undercooling. The width of the primary arms also decreases with large K, leading to the needle-like dendrite structures as shown in fig. 2. The volume fraction of the primary dendrite arm in the whole dendrite structure is also plotted in fig. 4(a), and large K would restrain the secondary arm developing, which would lead to the increasing fraction of the primary arm in the whole dendrite. It is well established that the dendritic microstructure could be greatly changed with different undercooling, since the microstructure is mainly determined by the crystallization rate as well as the atomic diffusion rate, which would be highly influenced by the temperature.

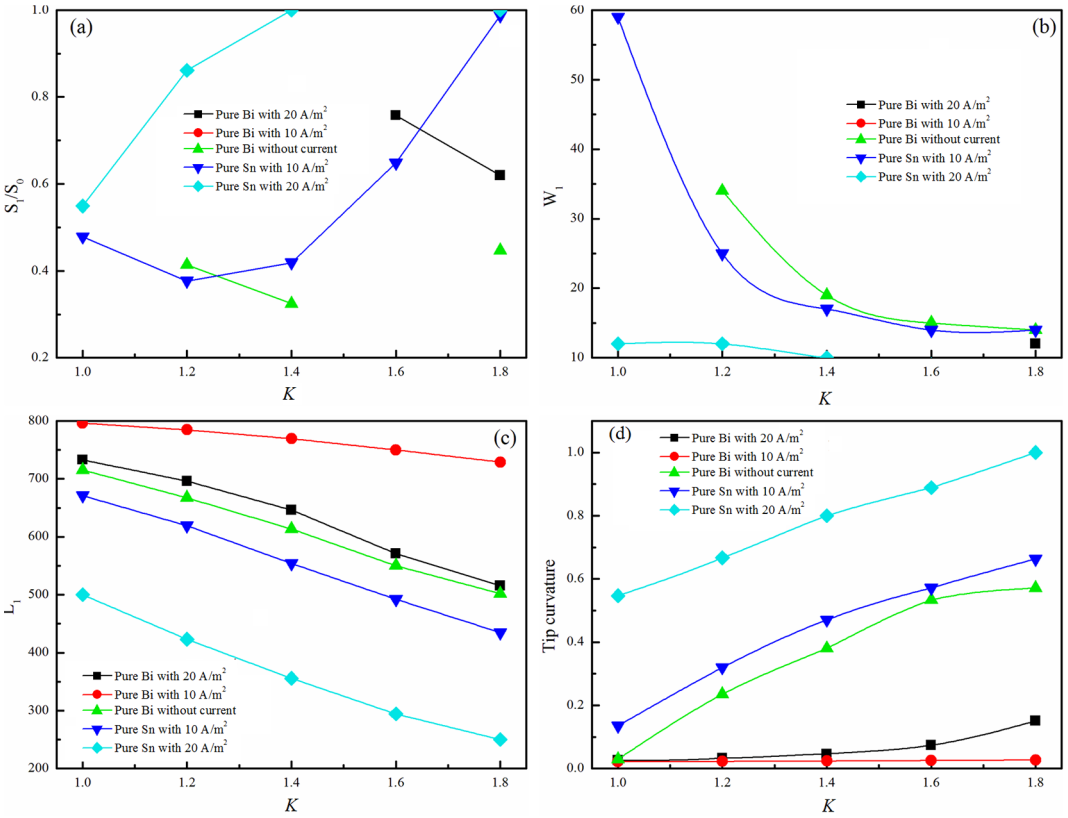

Fig. 4. Characteristics of the primary dendrite arms: (a) volume fraction of the primary arms in the whole dendrite; (b) width of the primary arm; (c) length of the primary arm; (d) tip curvature of the primary arm.

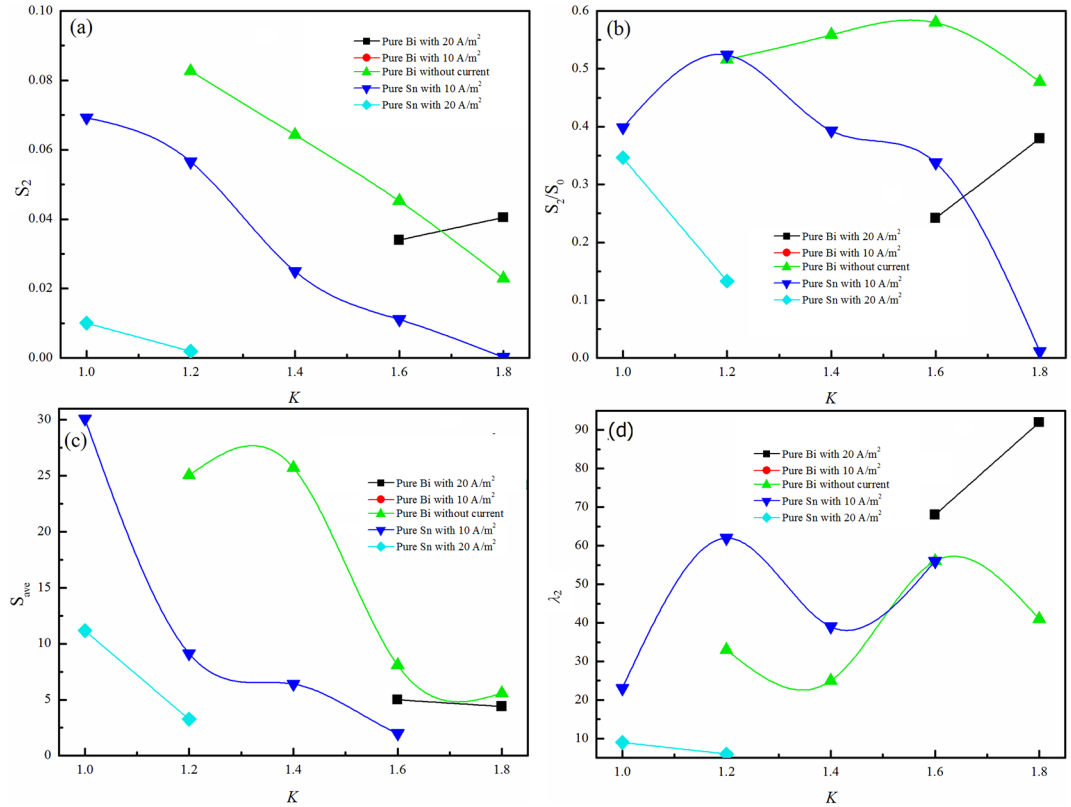

Fig. 5. Characteristics of the secondary dendrite arms: (a) volume of the secondary branches; (b) volume fraction of the secondary branches in the whole dendrite; (c) average volume of the secondary branches; (d) secondary dendrite arm spacing.

For solidifying with dendritic structures, the secondary dendrite arm spacing (SDAS, λ_2) is the most commonly characterized feature, since the SDAS has been found to be highly correlated to the strength and hardness of the metallic materials, and decreasing the SDAS would also reduce inter-dendritic shrinkage porosity, and influence electrical and thermal conductivity [22]. In fig. 5, the shape and distribution characteristics of secondary branches is plotted as a function of the K and current densities. The volume of the secondary branches would decrease with increasing K, since large heat extracting from the primary growing would lead to heat concentrating between primary arms, leading to reduced temperature undercooling which becomes the impaired effect on side-branches development. It should be noticed that for Bi with large current density ($20\,\mathrm{A/m^2}$), increasing K would result in side-branches developing. It has been proved that the SDAS is correlated to the crystallization rate and temperature gradient, and applying electric field would provide another way to control crystal structure.

4 Concluding remarks

It is of great importance to quantitatively determine the processing on the microstructure in metallic materials, which would give a better understanding of the mechanical behavior and microstructure details at the relevant length scales that contribute to this behavior. In this study, the sufficient characterization of dendritic structures is conducted upon the phase-field simulations on the dendritic formation with applied electric field. The thermoelectric effects as well as temperature undercooling on the dendrite structures are analyzed by implementing the image recognition technique. The shape characteristics as well as the number of the primary-, secondary- and higher-order branches are statistically analyzed for different pure substances. Results indicate that the side-branching development should be highly correlated to the temperature distributions near the growing interfaces, and the side-branching activities could be tailored by rationally controlling the applied electric filed as well the heat treatment, which could be a potential way to improve the mechanical properties in metallic materials.

This work was supported by the National Natural Science Foundation of China (grant numbers: 51501146, 51701152, 51705415), the Outstanding Youth Science Fund of Xi'an University of Science and Technology (grant number 2019YQ2-07), Project supported by enterprise joint fund of Shaanxi Natural Science Basic Research Program (grant number 2019JLM-11), Natural Science Foundation of Shaanxi Provincial Department of Education (grant number 8146119003).

Author contribution statement

Limei Fu performed the data analysis, and wrote the manuscript. Youqi Cao performed the simulations and revised the manuscript. Zhongtang Gao gave suggestion on the side-branching characteristic description. Lihong Dong performed the image data extraction. Lifei Du conceived the project and revised the manuscript.

References

1. M.E. Glicksman, A.O. Lupulescu, J. Cryst. Growth **264**, 541 (2004).
2. M. Asta, C. Beckermann, A. Karma, W. Kurz, R. Napolitano, M. Plapp, G. Purdy, M. Rappaz, R. Trivedi, Acta Mater. **57**, 941 (2009).
3. S. Shuai, E. Guo, Q. Zheng, M. Wang, T. Jing, Mater. Characterization **111**, 170 (2016).
4. R.B. Song, F.P. Dai, B.B. Wei, Sci. China: Phys. Mech. Astron. **54**, 901 (2011).
5. T.M. Wang, J.J. Xu, J. Li, W.X. Huang, S.C. Liu, T.J. Li, Sci. China: Technol. Sci. **53**, 1278 (2010).
6. K. Nagashio, K. Nozaki, K. Kuribayashi, Y. Katayama, Appl. Phys. Lett. **91**, 061916 (2007).
7. A. Karma, W.J. Rappel, Phys. Rev. E **57**, 4323 (1998).
8. F. Marinozzi, M. Conti, U.M.B. Marconi, Phys. Rev. E **53**, 5039 (1996).
9. R. Kobayashi, Physica D **63**, 410 (1993).
10. R.D. Doherty, E.A. Feest, K. Holm, Metall. Trans. **4**, 115 (1973).
11. L.L. Zheng, D.J. Larson, J. Cryst. Growth **180**, 293 (1997).
12. L. Du, R. Zhang, Integr. Mater. Manufacturing Innovat. **3**, 18 (2014).
13. L. Du, L. Zhang, P. Zhang, H. Du, Mater. Res. Express **4**, 076502 (2017).
14. L. Zhang, N. Li, H. Xing, R. Zhang, K. Song, L. Du, P. Yin, C. Yang, J. Cryst. Growth **430**, 80 (2015).
15. X. Liao, Q. Zhai, J. Luo, W. Chen, Y. Gong, Acta Mater. **55**, 3103 (2007).
16. J. Li, P. Ni, L. Wang, Y. Tan, Mater. Sci. Semicond. Process. **61**, 79 (2017).
17. Z. Xuan, F. Mao, Z. Cao, T. Wang, L. Zou, J. Alloys Compd. **721**, 126 (2017).
18. F. Yang, Z. Chen, F. Cao, R. Fan, H. Kang, W. Huang, Q. Yuan, T. Xiao, Y. Fu, T. Wang, J. Mater. Sci. Technol. **33**, 1134 (2017).
19. L.F. Du, Y.Q. Cao, Z.T. Gao, H.L. Du, Mater. Res. Express **5**, 096501 (2018).
20. S. Corre, T. Duffar, M. Bernard, M. Espezel, J. Cryst. Growth **180**, 604 (1997).
21. M.A. Tschopp, J.D. Miller, A.L. Oppedal, K.N. Solanki, Metall. Mater. Trans. A **45**, 426 (2013).
22. E. Vandersluis, C. Ravindran, Metallogr. Microstruct. Anal. **6**, 89 (2017).